05-4079

Final report of CONTACT NO: FA5209-04-P0441 REF: AOARD-04-4072

Mid-infrared MIS light emitter from strained Ge on Si with nano-structure enhancement

Prof. CheeWee Liu
Rm. 515, EE building II, Dept. of Electrical Engineering,
National Taiwan Univ. No.1, Sec.4, Roosevelt Rd. Taipei, 106 Taiwan
chee@cc.ee.ntu.edu.tw Tel: 886 2 23635251 ext. 515 Fax: 886 2 23638247

Abstract

The near-infrared emission was observed from Si/Ge heterojunction and Ge quantum dot metal-oxide-semiconductor light-emitting diodes, respectively. The 2-2.4 μm light emission is proposed to originate from the type-II Ge/Si heterojunction. i.e, the recombination of holes on the valence bandedge of the Ge quantum well and the electrons on the conduction bandedge of the Si cap. The infrared emission of ~1.5 μm was observed from Ge quantum dot metal-oxide-semiconductor light-emitting diodes, similar to p-i-n structure reported previously. At the negative gate bias, the electrons tunneling from Al gate electrode reach the semiconductor and recombine radiatively with holes. The electrons also recombine with holes in the Si cap and the bandedge emission from Si is also observed. The role of interface roughness and nano-structure is also be researched.

Related publication

1. M. H. Liao, C.-Y. Yu, C.-F. Huang, C.-H. Lin, C.-J. Lee, M.-H. Yu, S. T. Chang, C.-Y. Liang, C.-Y Lee, T.-H. Guo, C.-C. Chang, and C. W. Liu, "2 μm emission from Si/Ge heterojunction LED and up to 1.55 μm detection by GOI detectors with strain-enhanced features" accepted by IEDM, 2005
2. M. H. Liao, C.-Y. Yu, T.-H. Guo, C.-H. Lin, S. T. Chang, C.-T. Chia, and C. W. Liu, "Electroluminescence from the Ge quantum dot metal-oxide-semiconductor tunneling diodes" submitted to *IEEE Electron Device Lett.*, 2005.

Report Documentation Page

Form Approved
OMB No. 0704-0188

Public reporting burden for the collection of information is estimated to average 1 hour per response, including the time for reviewing instructions, searching existing data sources, gathering and maintaining the data needed, and completing and reviewing the collection of information. Send comments regarding this burden estimate or any other aspect of this collection of information, including suggestions for reducing this burden, to Washington Headquarters Services, Directorate for Information Operations and Reports, 1215 Jefferson Davis Highway, Suite 1204, Arlington VA 22202-4302. Respondents should be aware that notwithstanding any other provision of law, no person shall be subject to a penalty for failing to comply with a collection of information if it does not display a currently valid OMB control number.

1. REPORT DATE	2. REPORT TYPE	3. DATES COVERED
20 NOV 2007		

4. TITLE AND SUBTITLE	5a. CONTRACT NUMBER
Mid-infrared (2 ï¿½ 4μm) MIS light emitter from strained Ge on Si with nano-structure enhancement	**FA520905P0473**
	5b. GRANT NUMBER
	5c. PROGRAM ELEMENT NUMBER

6. AUTHOR(S)	5d. PROJECT NUMBER
Cheewee Liu	5e. TASK NUMBER
	5f. WORK UNIT NUMBER

7. PERFORMING ORGANIZATION NAME(S) AND ADDRESS(ES)	8. PERFORMING ORGANIZATION REPORT NUMBER
National Taiwan University,No 1 Sec 4 Rooselvelt,Taipei,Taiwan,TW,106	**N/A**

9. SPONSORING/MONITORING AGENCY NAME(S) AND ADDRESS(ES)	10. SPONSOR/MONITOR'S ACRONYM(S)
	11. SPONSOR/MONITOR'S REPORT NUMBER(S)

12. DISTRIBUTION/AVAILABILITY STATEMENT

Approved for public release; distribution unlimited.

13. SUPPLEMENTARY NOTES

14. ABSTRACT

This project involved the observations of near-infrared emissions from Si/Ge heterojunctions and Ge quantum dot metal-oxide-semiconductor light-emitting diodes.

15. SUBJECT TERMS

16. SECURITY CLASSIFICATION OF:			17. LIMITATION OF ABSTRACT	18. NUMBER OF PAGES	19a. NAME OF RESPONSIBLE PERSON
a. REPORT	b. ABSTRACT	c. THIS PAGE		**25**	
unclassified	**unclassified**	**unclassified**			

I. Introduction

It attracts the great attention to investigate semiconductor devices emitting in the wavelength of $2-5\mu m$ mid-infrared spectral region, including strained InGaAsSb quantum well lasers at 2.7 μm up to room temperature [1], quantum cascade lasers [2-3], conventional narrow band gap interband lasers [4], and InAs/AlSb quantum cascade intersubband light-emitting devices [5]. The most common material systems used for the light-emitting technology are III-V-based systems. However, due to the compatibility with Si technology, the Si-based light emitters are the holy grails [6] in this research area for the full integration of electrical and optical devices. The bandedge light emission of ~1.1 μm wavelength from Si metal-oxide-semiconductor (MOS) diode was reported by our group for years [7-10]. To extend the emission wavelength, the Si/Ge heterojunction and Ge quantum dot MOS diode with bandedge light emission is reported in this work.

II. 2 μm emsiion from Si/Ge heterojunction LED

The epi Ge layer (~4 nm) is directly grown on Si (100) at 525 $°C$ by ultra-high-vacuum chemical vapor deposition (UHV/CVD). To improve the interface between the oxide and the epi Ge, a Si cap is grown on the top of Ge for passivation and forms the Ge quantum well. The 2 nm oxide is used for the tunneling oxide grown by liquid phase deposition (LPD) at 60 $°C$ to allow the carrier transport from the electrode to the semiconductor. Due to the traps in LPD oxide, the trap-assistant tunneling current is

dominant in the 2 nm thick LPD oxide [11]. The diodes have Al gate electrodes with the circular area defined by the shadow mask. Another Al contact is on the back of the wafer.

Fig. 1 shows the cross-sectional micrograph of transmission electron microscopy (TEM) image of ~4 nm Ge quantum well with ~1 nm Si cap on the Si (100) wafer. No apparent defect is observed in these layers. Fig. 2 shows Raman spectra excited by the 514 nm Ar laser for the Ge quantum well on Si (curve 1) and bulk Si (curve 2). Since the bulk Si has the signal of ~300 cm^{-1} close to Ge signal, the Raman spectrum of the pure Ge layer on Si is obtain from the subtraction of the bulk Si signal from the measured spectrum of the Ge quantum well on Si. Note that due to thin Si cap (1 nm), its signal is too weak to be measured. The resulting Raman spectrum of pure epi Ge without Si substrate interference has a broad feature located at ~304.1 cm^{-1} (curve 3 in Fig. 2). As compared with the bulk Ge (curve 4), the Raman shift of Ge-Ge phonon frequency ($\Delta\omega_{Ge\text{-}Ge}$) of the Ge quantum well with respect to the bulk Ge peak can be determined (4.4 cm^{-1}). Note that Lorentzian line shape was used to determine the peak position of the line shape. The shift is due to the strain and the phonon confinement in the Ge quantum well [12, 13] and is given by :

$$\Delta\omega = \frac{1}{2\omega_0}[p\varepsilon_{zz} + q(\varepsilon_{xx} + \varepsilon_{yy})] \quad (1)$$

$$\varepsilon_{zz} = -(2C_{12})/(C_{11})\varepsilon_{xx},\ \ \varepsilon_{xx} = \varepsilon_{yy} \quad (2)$$

where ω_0 is the longitudinal phonon frequency at the zone center of reciprocal space, p and q are Ge deformation potentials, ε_{xx}, ε_{yy}, ε_{zz} are the strain, and C_{11}, C_{12} are elastic

coefficients. Using the Raman shift (~4.4 cm^{-1}) of Ge-Ge phonon of the Ge quantum well, and the phonon confinement model [14], the biaxial compressive strain ($\varepsilon_{xx} = \varepsilon_{yy}$) in the Ge quantum well is estimated.

Fig. 3 shows the electroluminescence (EL) spectra at different temperatures from the Ge quantum well MOS light emitting diode (LED) with 1 nm Si cap and the device size of 4×10^{-2} cm^2. The drive current is 50 mA at the gate voltage of -8 V. The electron-hole-plasma (EHP) recombination model [15] can be used to fit the EL spectra. Device temperatures of 130 K, 210 K, and 320 K are obtained from the fitting of the EL line shapes, while the corresponding temperatures of cold finger in the EL measurement are 10 K, 150 K, and 300 K. The temperature difference is due to the device heating [16]. The width of the emission peak increases with the increasing temperature due to the wide distribution in energy of electrons and holes at high temperature. The apparent bandgap extracted by the EHP model is ~0.52 eV (~2.4 μm) and ~0.56 eV (~2.2 μm) at the temperature of 320 K and 130 K, respectively. The apparent bandgap is the low energy edge of the emission peak in the spectra.

Using the formula in Ref. 17, 18 and the parameters in Ref. 19, the band diagram of Al/SiO_2/p-type semiconductor at the accumulation bias at 320 K is shown in Fig. 4. The strained Ge/Si substrate junction is type-II alignment with $\Delta E_C = 0.19$ eV and $\Delta E_V = 0.76$ eV. The cap Si/strained Ge junction is also type-II alignment with $\Delta E_C = 0.15$

eV and $\Delta E_V = 0.36$ eV. To determine the possible origin of ~0.52 eV emission, the quantum confinement energy of the Si cap and the Ge quantum well are calculated. With the assumption of a triangular potential profile in the Si cap and a square potential profile in the Ge quantum well, the quantum confinement energy of 100 meV is found in the conduction bandedge of strained Si cap, 110 meV is in the valence bandedge of strained Si cap, and 60 meV is in the valence bandedge of Ge quantum well, using the electron (hole) effective mass of 0.19 m_o (0.16 m_o) in the Si cap, and the hole effective mass of 0.28 m_0 in the Ge quantum well. At negative bias, the electrons tunnel from the Al gate to the semiconductor and the holes also tunnel from the semiconductor to Al gate. However, the dominant gate current is the electron tunneling current due to lower electron tunneling barrier as compared to holes (3.1 eV vs 4.6 eV). Meanwhile, the negative gate bias also accumulates holes in the valence bandedge of strained Si cap and the Ge quantum well. Due to type-II band alignment at the strained Ge/Si heterostructure, the electrons in the Si cap can recombine with the holes in Ge quantum well, giving a theoretic emission edge of ~0.56 eV. There are 40 meV reduction between the theoretic value (~0.56 eV) and the measured data (~0.52 eV). The possible explanation of the difference are the surface bending, the Ge phonon of 36 meV emission in the light-emission process [20], the bandgap narrowing at high carrier density [21] and the interdiffusion of Si into Ge quantum well during the Si cap growth [17]. The first three mechanisms can reduce the photon

emission energy, but the last mechanism increases the photon emission energy. Note that the direct recombination of electrons and holes in the Ge quantum well gives the photon energy of ~0.61eV (Fig. 4), which is much larger than the experimental data of 0.52 eV.

III. Electroluminescence from the Ge quantum dot metal-oxide-semiconductor tunneling diodes

The Si/Ge QDs are prepared by ultra-high-vacuum chemical vapor deposition (UHV/CVD) on p-type Si (001) substrates with resistivity of 15-25 $\Omega-cm$. After Si buffer layer of 100 nm was grown, 20 periods of Ge/Si bilayers were grown to form the self-assembled Ge QDs at temperature of 600 °C under the Stranski-Krastanov (SK) growth mode [22]. The Ge layers are separated by 60 nm Si spacer layers. A 3 nm (nominal thickness) Si cap was deposited above the top layer of self-assembled Ge layer as a cap layer for the subsequent deposition of liquid phase deposition (LPD) oxide. The undoped Si/Ge layers has a background hole concentration of ~1 x 10^{14} cm^{-3}. To avoid material degradation such as strain relaxation and Ge out diffusion, the low temperature oxide (LPD oxide) is used to reduce the thermal budget of SiGe device process [23]. The traps in the LPD oxide and small thickness (~2 nm) allow the significant tunneling electrons to inject into semiconductor from Al electrode. At negative bias, the electrons tunnel from the Al gate to the substrate and the holes also tunnel from the substrate to Al gate. However, due to the different barrier heights between electrons (~3.1 eV) and holes (~4.6 eV), the hole

current is smaller than the electron current. Meanwhile, the negative gate bias also attracts holes in the p type semiconductor, and the tunneling electrons can recombine with holes at the oxide/Si interface and in the Ge QD to emit ~1.1 μm and ~1.5 μm infrared, respectively. The diodes have Al gate electrodes with the circular area defined by the shadow mask. Another Al contact is on the back of the wafer.

The surface morphology of LPD oxide deposited on Ge QDs is shown in Fig. 5(a). The tensile strain field on the Si cap of self-assembled QDs can have preferential oxide deposition during LPD process. The oxide dots are formed on the tensile strained area of Si cap, and are aligned vertically with Ge QDs embedded in the Si caps [24]. Fig. 5(b) shows the cross-section transmission electron microscopy (TEM) image of the 20-period Ge QDs structure with the base and the height of ~120 nm and ~7nm, respectively. The area density of Ge islands is about 4 x 10^9 cm^{-2}. Fig. 6 shows Raman spectra excited by the 514 nm Ar laser for the Ge QD, bulk Ge, and bulk Si. Besides the strong Si substrate signal at 520 cm^{-1}, Ge-Ge, Si-Ge, and local Si-Si vibrational peaks can be seen at about 302, 417, and 436 cm^{-1}, respectively. The appearance of the Si-Ge and local Si-Si vibrational peak implies the formation of SiGe alloy in the wetting layers [25]. On the other hand, the Ge-Ge peak is most possibly contributed by the islands [25]. As compared with the bulk Ge, the Raman shift of Ge-Ge phonon frequency of the Ge QD with respect to the bulk Ge peak can be determined (~2 cm^{-1}). The possible factors responsible to this frequency shift are the

alloying of the Ge QDs with Si spacers, the phonon confinement effect in the QDs, and the effects of compressive strain. The first two mechanisms reduce the phonon frequency, but the last mechanism increases the phonon frequency. It is reported that the Ge-Ge peak position of strained Ge or Ge_xSi_{1-x} with x>0.7 should be larger than 306 cm^{-1} [26,27]. Therefore, the downward shift of Ge-Ge peak to 302 cm^{-1} in Fig. 2 is mainly attributed to the phonon confinement in addition to the effects of strain and alloying.

Figure 7 shows the photoluminescence (PL) spectra at different temperatures from the Ge QD at a pump power of 60 W/cm^2. There are two PL peaks located at ~1.1 eV and ~0.85 eV. These two peaks are most likely from the optical transitions related to the Si substrate and Ge QD [28]. Figure 8 shows the electroluminescence (EL) spectra at different temperature from the Ge QD MOS LED samples with the device size of 4 x 10^{-2} cm^2. The drive current is 100 mA at the gate voltage of -8 V. Device temperatures of ~340 K, ~250 K, ~160 K, and ~110 K are obtained from fitting of the EL line shapes [16], while the temperatures of the cold finger in the EL measurement are 300 K, 200 K, 100 K, and 10 K, respectively. The temperature difference is due to the device heating. The band diagram of Ge QD MOS LED at the accumulation condition is shown in the inset of Fig. 8. The tunneling current of electrons at the negative bias can cause electron hole recombination at the oxide/Si interface and in the Ge QDs to emit ~1.1 μm and ~1.5 μm infrared. The EL spectrum of similar Ge QD p-i-n diode is also shown for the reference. The infrared

emission of ~1.5 μm observed from Ge QD MOS LED is similar to p-i-n structure reported previously [29]. However, no ~1.1 μm light emission was observed in the conventional Ge QD p-i-n diode. The electron and hole recombine mainly in the Ge QD and the built-in field in the depletion region renders the holes hard to capture the electrons in the i layers. Note that for MOS LED, there are a lot of holes accumulated at oxide/Si interface to recombine with electrons. The experimental setup to apply external strain on Ge QD MOS LED is similar to Ref. 30 and Ref. 31. The Si energy gap extracted by the light emission spectra at the temperature of 110 K from the relaxed device is reduced by 15 meV under 0.13% biaxial tensile strain measured by Raman spectroscopy [30]. However, the blue shift (~12 meV) of EL spectra at 110 K was found in the Ge QD (Fig. 9). The red shift of the bulk Si is due to the downshift of conduction band and the upshift of the valence band. The blue shift of the Ge QD is due to the downshift of both Ge conduction band and Ge valence band. The blue shift is the difference of these two downshifts. Note the original compressive strain in Ge decreases by the external tensile strain. The decrease of the compressive strain increases the band gap as compared to the original Ge QD without external strain.

IV. Roughness-Enhanced Electroluminescence from Metal Oxide Siliocn Tunneling Diodes

To further investigate the roughness effect on the oxide reliability, the light

emission intensity at bandgap energy is measured. The time evolutions of emission intensity from the flat and the rough PMOS diodes are shown in Fig. 10. The operation gate current is 100 mA and the device area is 150 cm^2. The intensity of the rough devices shows very slight variation during the stress time, while that of the flat devices degrades about 15% after 1200 s stress. The degradation of bandgap light emission indicates the formation of interface states, which act as nonradiative recombination centers. The interface states may be induced due to the breakage of the Si-H bonds by injected holes. The stress of hole current generates more interface states in the flat oxide than in the rough oxide. The rough oxide is more robust to tunneling carrier stress than the flat oxide, since the momentum energy of the injected hole tunneling from Al gate is scattered by the oxide roughness, and this lowers the injected hole momentum perpendicular to the interface to bombard the Si/oxide interface. The light emission of NMOS diodes showed similar results. Fig. 11 shows the speculative mechanism of the roughness enhanced oxide reliability in PMOS tunneling diodes. When the carriers tunnel through the oxide, they are scattered by the oxide roughness and the momentum of the injected holes perpendicular to the interface is reduced. In the PMOS tunneling diodes, the oxide degradation is related to the tunneling hole induced traps in bulk oxide, and the threshold energy for the injected holes to be captured by O vacancy is 1.8 eV. This indicates that only the hole with injected energy higher than 1.8 eV. Can be trapped in the oxide and can induce oxide degradation. Since the

reliability of the MOS tunneling diode is related to the energy of the injected holes, the perpendicular energy reduction of the holes tunneling through the oxide could improve the electrical and optical reliability of the devices. However, it is an intuitive model, and more evidence is needed to give a clear picture of the phenomenon.

V. CONCLUSION

The near-infrared emission is observed from the MOS LED. The origin of the emission is due to the radiative recombination between the electrons in the cap Si layer and the holes confined in the Ge quantum well. The large strain can possibly further extend the wavelength to mid-infrared for the radiative recombination at Si/Ge type II interface. On the other hand, the ~1.5 μm Ge QD MOS LED is reported for the first time. The origin of the emission is due to the radiative recombination between the electrons and holes confined in the Ge QD. The electrons also recombined with holes at the Si/oxide interface and the band edge emission from Si is also observed, while Si emission was not observed in the conventional p-i-n LED. By the proper design of the strain mechanism, it can possibly further tune the wavelength for the light emission. The rough oxide can be a novel technology to improve both the electrical and optical reliability of MOS devices.

References

1. D. Garbuzov, H. Lee, V. Khalfin, R. Martinelli, J. C. Connolly, and G. L. Belenky, IEEE Photonics Technol. Lett. 11, 794 (1999).

2. R. Kohler, C. Gmachl, A. Tredicucci, F. Capasso, D. L. Sivco, S. N. G. Chu, and A. Y. Cho, *Appl. Phys. Lett*, 76, 1092 (2000).

3. J. Faist, F. Capasso, D. L. Sivco, A. L. Hutchinson, S. G. Chu, and A. Y. Cho, *Appl. Phys. Lett*, 72, 680 (1998).

4. J. C. Kim, L. Shterengas, R. U. Martinelli, G. L. Belenky, D. Z. Garbuzov, and W. K. Chan, *Appl. Phys. Lett*, 81, 3146 (2002).

5. C. Becker, I. Prevot, X. Marcadet, B. Vinter, and C. Sirtori, *Appl. Phys. Lett*, 78, 1029 (2001).

6. *IEEE Spectrum,* 41, 27 (2004).

7. C. W. Liu, M. H. Lee, C. F. Lin, I. C. Lin, W. T. Liu, and H. H. Lin, Tech. Dig., Int. Electron Device Meeting, 749 (1999).

8. C. W. Liu, M. H. Lee, M.-J. Chen, C.-F. Lin, and M. Y. Chern, *IEEE Electron Device. Lett.*, 21, 601 (2000).

9. C. W. Liu, C.-H. Lin, M. H. Lee, S. T. Chang, Y.-H. Liu, M.-J. Chen, and C.-F. Lin, *Appl. Phys. Lett*, 78, 1937 (2001).

10. T. C. Chen, W. Z. Lai, C. Y. Liang, M. J. Chen, L. S. Lee, and C. W. Liu, J. Appl. Phys.

95, 6486 (2004).

11. K.-C. Lee and J.-G. Hwu, *IEEE Electron Device. Lett.*, 18, 565 (1997).

12. Y. Hida, T. Tamagawa, H. Ueba, and C. Tatsuyama, J. Appl. Phys. 67, 7274 (1990).

13. J. L. Liu, J. Wan, Z. M. Jiang, A. Khitun, K. L. Wang, and D. P. Yu, J. Appl. Phys. 92, 6804 (2002).

14. M. Ichimura, A. Usami, A. Wakahara, and A. Sasaki, J. Appl. Phys. 77, 5144 (1995).

15. C. W. Liu, M. H. Lee, M.-J. Chen, I. C. Lin, and C.-F. Lin, *Appl. Phys. Lett*, 76, 1516 (2000).

16. C. W. Liu, M.-J. Chen, I. C. Lin, M. H. Lee, and C.-F. Lin, *Appl. Phys. Lett*, 77, 1111 (2000).

17. Chris G. Van de Walle, Physical Review B, 34, 5621 (1986).

18. Chris G. Van de Walle, Physical Review B, 39, 1871 (1989).

19. EMIS Datareviews Series No.20 "Properties of Crystalline Silicon" edited by Robert Hull (1999).

20. J. Weber and M. I. Alonso, Physical Review B, 40, 5683 (1989).

21. Y. Taur and T. H. Ning, *Fundamentals of Modern VLSI Devices* (Cambridge University Press, New York, 1998), p. 300.

22. T. I. Kamins, D. A. A. Ohlberg, R. S. Williams, W. Zhang, and S. Y. Chou, *Appl. Phys. Lett.* vol. 74, pp. 1773-1775, 1999.

23. B.-C. Hsu, S. T. Chang, C.-R. Shie, C.-C. Lai, P. S. Chen, and C. W. Liu, in *IEDM Tech.*

Dig., pp. 91-94, 2002.

24. C. W. Liu, B.-C. Hsu, K.-F. Chen, M. H. Lee, C.-R. Shie, and P.-S. Chen, *Appl. Phys. Lett.* vol. 82, pp. 589-591, 2003.

25. J. L. Liu, Y. S. Tang, K. L. Wang, T. Radetic, and R. Gronsky, *Appl. Phys. Lett.* vol. 74, pp. 1863-1865, 1999.

26. W. J. Brya, *Solid-State Communications* vol. 12, pp. 253-257, 1973.

27. F. Cerdeira, A. Pinczuk, J. C. Bean, B. Batlogg, and B. A. Wilson, *Appl. Phys. Lett.* vol. 45, pp. 1138-1140, 1984.

28. L. P. Rokhinson, D. C. Tsui, J. L. Benton, and Y.-H. Xie, *Appl. Phys. Lett.* vol. 75, pp. 2413-2415, 1999.

29. Y. H. Peng, C.-H. Hsu, C. H. Kuan, C. W. Liu, P. S. Chen, M.-J. Tsai, and Y. W. Suen, *Appl. Phys. Lett.* vol. 85, pp. 6107-6109, 2004.

30. M. H. Liao, M.-J. Chen, T. C. Chen, P.-L. Wang, and C. W. Liu, *Appl. Phys. Lett.* vol. 86, p. 223502, 2005.

31. M. H. Liao, C.-Y. Yu, C.-F. Huang, C.-H. Lin, C.-J. Lee, M.-H. Yu, S. T. Chang, C.-Y. Lee, T.-H. Guo, C.-C. Chang, and C. W. Liu, accepted by *IEDM Tech. Dig.*, 2005.

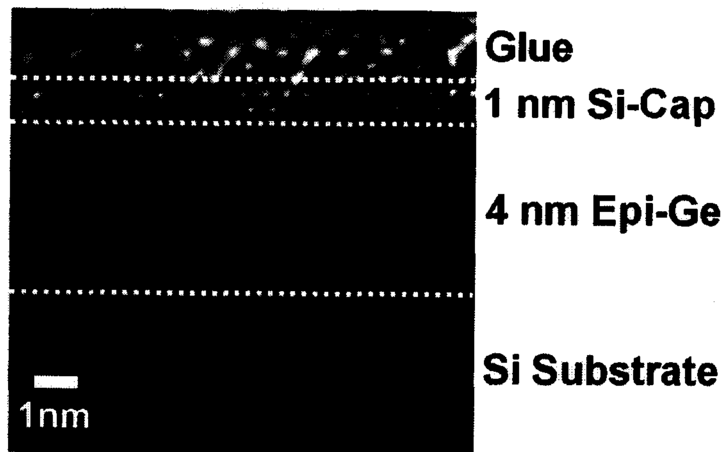

Fig. 1 The cross-sectional transmission electron micrograph of the as-grown Ge quantum well on (100) Si.

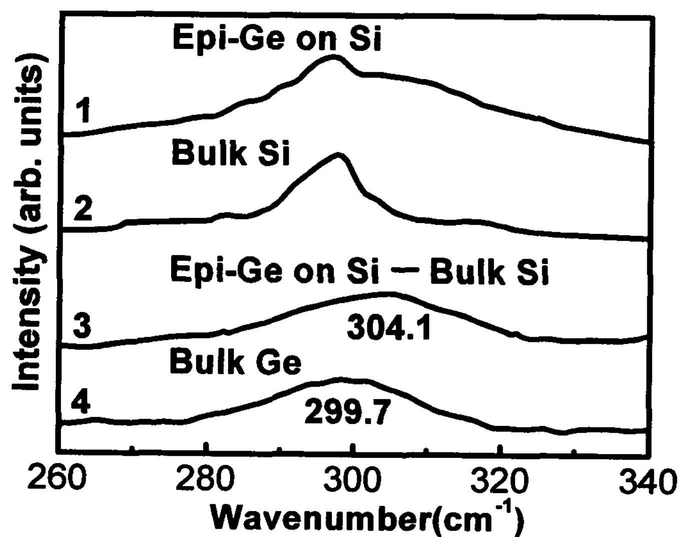

Fig. 2 The Raman spectrum of Ge quantum well on Si (curve 1). Curve 2 is the Raman spectrum of the Si substrate. The Raman spectrum of the pure Ge layer without Si substrate interference is shown in the curve 3. The spectrum of the bulk Ge wafer (curve 4) is shown for reference. The blue wavenumber shift of Ge-Ge peak of the pure Ge layer without Si substrate interference with respect to the bulk Ge indicates the compressive strain.

Wavelength(μm)
2.4 2.2 2.0 1.8 1.2 1.0
EL Intensity (arb. unit)
Data
Fit
~130K
~210K
~320K
0.5 0.6 0.7 1.0 1.1 1.2
Energy gap(eV)

Fig. 3 The measured electroluminescence (EL) spectra of strained Ge/Si quantum well metal-oxide-silicon light-emitting diode (MOS LED) with the fitting curves of the electron-hole plasma recombination model at 130 K, 210 K, and 320 K..

−
+
0.15eV
0.19eV
CB
hν
0.61eV
0.76eV
0.36eV
VB
Al
SiO_2
Si
Ge
p-Si

Fig. 4. The schematic band diagram of the strained Ge quantum well (4 nm) device with a Si cap (1 nm) for NMOS tunneling diode.

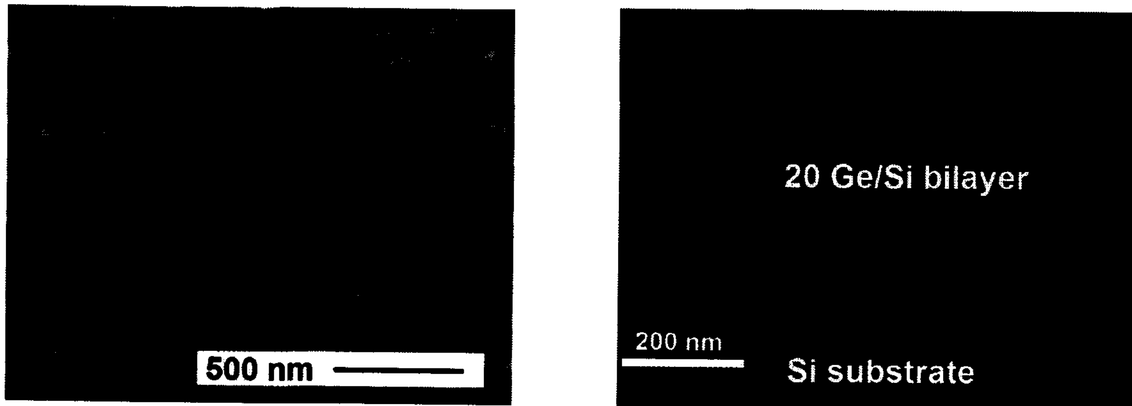

Fig. 5 (a) AFM surface image of liquid phase deposition oxide on the Si cap layer of 20-period self-assembled Ge quantum dot (QD) sample with 60 nm Si spacers; (b) Cross-Section TEM micrograph of the self-assembled Ge QDs structure.

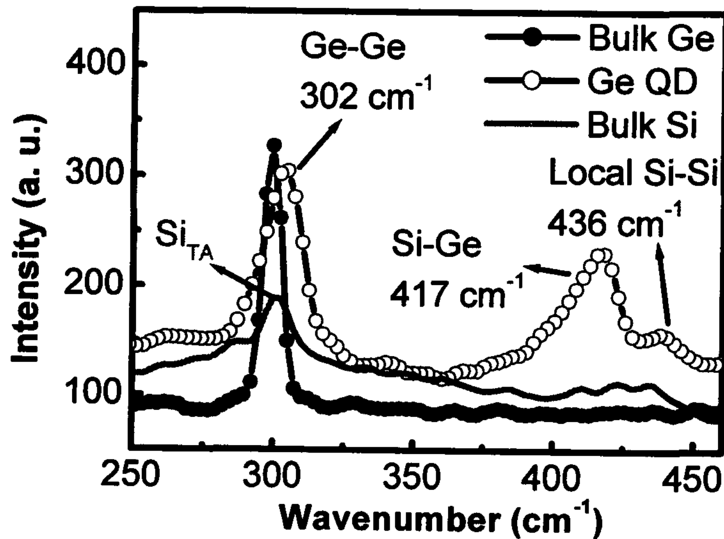

Fig. 6 The Raman spectra of bulk Si, bulk Ge, and Ge QD. Ge-Ge, Si-Ge, and local Si-Si optical modes can be found at around 302 cm^{-1}, 417 cm^{-1}, and 436 cm^{-1}, respectively.

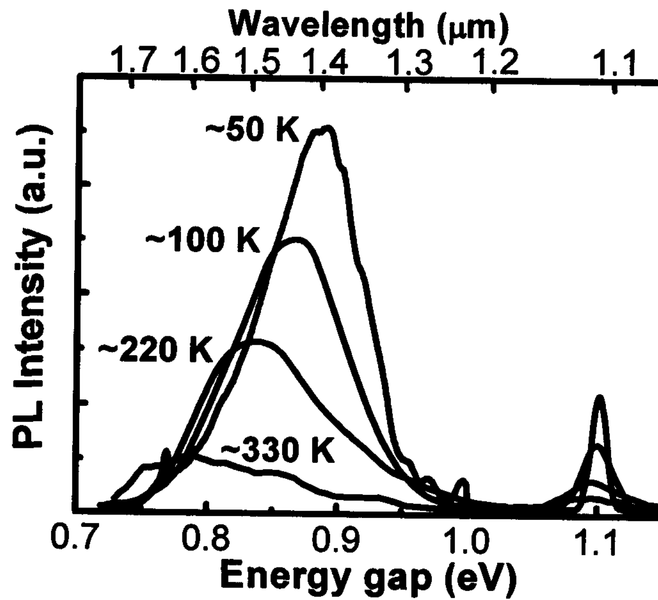

Fig. 7 Photoluminescence (PL) spectra of the Ge QD at different temperature. The infrared emission of ~1.1 μm and ~1.5 μm was observed from the transition of Si and the Ge QD.

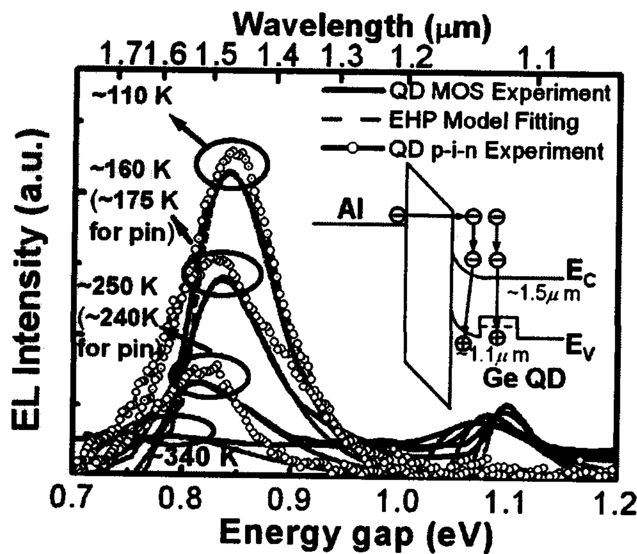

Fig. 8 Electroluminescence (EL) spectra of the Ge QD MOS light emitting diode (LED) at different temperatures with the fitting curves of the electron-hole-plasma recombination model. The inset shows the energy band diagram of the Ge QD MOS LED at the accumulation bias. The EL spectra of Ge QD p-i-n diode is also shown for reference.

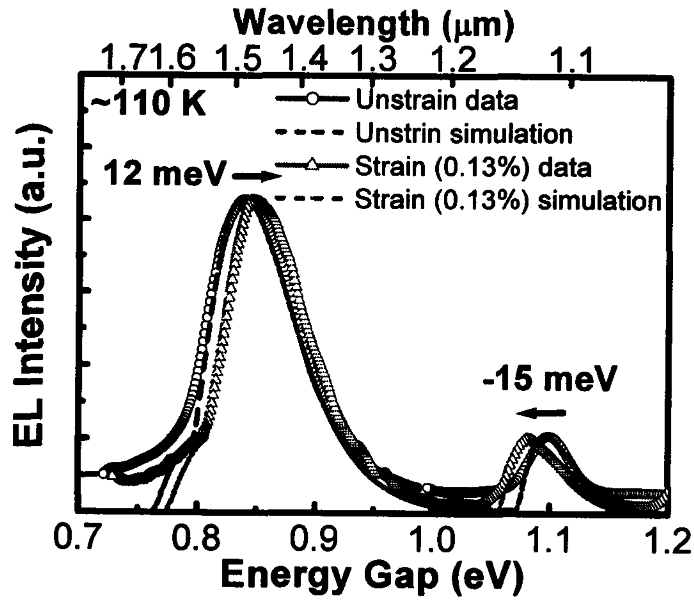

Fig. 9 Measured EL spectra of relaxed/strained Ge QD MOS LED (0.13% strain measured by Raman spectroscopy) with the fitting curves of the electron-hole plasma recombination model at ~110 K.

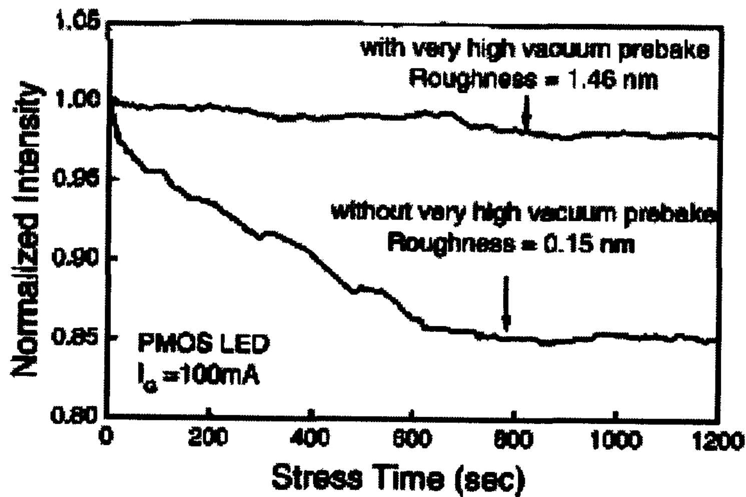

Fig. 10 Time evolutions of light emission intensity from the flat and the rough PMOS diodes. The rough PMOS diode shows much less emission intensity degradation than the flat PMOS device.

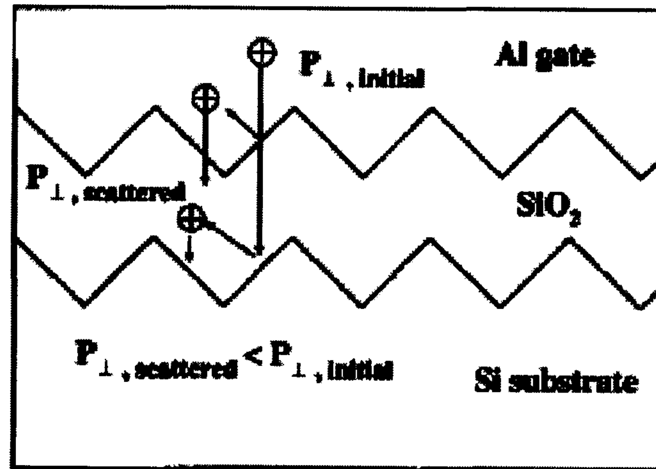

Fig. 11 Illustration of the speculative mechanism of the roughness enhanced reliability. The hole impact energy perpendicular to the Si/SiO_2 and Al/SiO_2 interface is reduced due to the surface and interface roughness scattering. The multiple scattering of the tunneling hole are possible in this process.

Paper generated that contain an AFOSR/AOARD acknowledgement

1. M. H. Liao, C.-Y. Yu, C.-F. Huang, C.-H. Lin, C.-J. Lee, M.-H. Yu, S. T. Chang, C.-Y. Liang, C.-Y Lee, T.-H. Guo, C.-C. Chang, and C. W. Liu, "2 μm emission from Si/Ge heterojunction LED and up to 1.55 μm detection by GOI detectors with strain-enhanced features" accepted by IEDM, 2005

2. M. H. Liao, C.-Y. Yu, T.-H. Guo, C.-H. Lin, S. T. Chang, C.-T. Chia, and C. W. Liu, "Electroluminescence from the Ge quantum dot metal-oxide-semiconductor tunneling diodes" submitted to *IEEE Electron Device Lett.*, 2005.

Appendix:

M. H. Liao, C.-Y. Yu, C.-F. Huang, C.-H. Lin, C.-J. Lee, M.-H. Yu, S. T. Chang, C.-Y. Liang, C.-Y Lee, T.-H. Guo, C.-C. Chang, and C. W. Liu, "2 μm emission from Si/Ge heterojunction LED and up to 1.55 μm detection by GOI detectors with strain-enhanced features" accepted by IEDM, 2005.

2 μm emission from Si/Ge heterojunction LED and up to 1.55 μm detection by GOI detectors with strain-enhanced features

M. H. Liao[a], C.-Y. Yu[a], C.-F. Huang[a], C.-H. Lin[a], C.-J. Lee[a], M.-H. Yu[a], S. T. Chang[b], C.-Y. Liang[a], C.-Y. Lee[a], T.-H. Guo[a], C.-C. Chang[a], and C. W. Liu[a]*

[a] Department of Electrical Engineering, Graduate Institute of Electronics Engineering, and Graduate Institute of Electro-Optical Engineering, National Taiwan University, Taipei, Taiwan, R. O. C.

[b] Department of Electrical Engineering, National Chung Hsing University, Taichung, Taiwan, R. O. C.

*E-mail: chee@cc.ee.ntu.edu.tw

Abstract

The Ge/Si heterojunction MOS LED can emit ~2 μm light due to the radiative recombination at type II heterojunction. The fully depleted 800 nm germanium on insulator (GOI) can increase the responsivity and the speed of the MOS detector due to the large absorption of Ge and the electrical field in the active layer, respectively. Moreover, the external strain can tune the emission energy (~11 meV) by modifying the band structure. The responsivity of GOI MOS detector is also improved by ~10% using the external strain. Both heterojunction and strain (internal or external) can enhance the performance of Si-based optoelectronics.

Introduction

Due to the compatibility with Si technology, the Si-based optoelectronic devices are the holy grails for the full integration of electrical and optical devices. The band edge light emission of ~1.1 μm wavelength from the Si MOS LED [1] and the high efficient Ge quantum dot MOS photodetector [2] were reported in the past. The electroluminescence (EL) of MIS structure is an effective indicator of Dit at the interface and the strain level in the Si channel by its intensity and energy position, respectively [3-4] for the future in-line inspection tool. In this paper, the mid-infrared emission of 2 to 2.4 μm is observed from Si/Ge heterojunction MOS LED for the fist time and can be used for the detection of the explosives. To increase the responsivity of Si-based detectors, the thick Ge to increase the absorption is necessary. The thick epi-Ge on Si leads to high defect density, which significant traps the photo-generated carriers. The bulk Ge has less defect density and can be transferred to Si or SOI substrates by smart cut and wafer bonding. The resulting GOI photodetector has the high responsivity and speed. Besides the mobility enhancement by strain [5], the optical absorption can be also enhanced by the strain to increase the detector responsivity. The strain, heterojunction, and Ge layer transfer can boost the optoelectronic performance of Si devices.

Fabrication and Characterization

The Ge quantum well (~4 nm) for light emitting diode was directly grown on Si (100) at 525 °C by ultra-high-vacuum chemical vapor deposition (UHV/CVD). A passivated Si layer (~1 nm) was capped on epi-Ge layer to improve the interface between oxide and epi-Ge layer (Fig. 1(a)). The 2 nm oxide used for the tunneling oxide was grown by liquid phase deposition (LPD) at 60 °C to allow the carrier tunneling between the electrode and the semiconductor. Before oxidation, the sample was cleaned by a HF dip. The Al or Pt circular gate electrodes with various areas are defined by the shadow mask. Fig. 1(b) shows Raman spectra excited by the 514 nm Ar laser for the Ge quantum well on Si (curve 1) and bulk Si (curve 2). Since the bulk Si has the signal of ~300 cm^{-1} close to Ge signal, the Raman spectrum of the pure Ge layer on Si is obtained from the subtraction of the bulk Si signal from the measured spectrum of the Ge quantum well on Si. Note that the signal of thin Si cap (1 nm) is too weak to be measured. The resulting Raman spectrum of pure epi Ge without Si substrate interference has a broad feature located at ~304.1 cm^{-1} (curve 3 in Fig. 1(b)). As compared with the bulk Ge (curve 4), the Raman shift of Ge-Ge phonon frequency ($\Delta\omega_{Ge-Ge}$) of the Ge quantum well with respect to the bulk Ge peak can be determined (~4.4 cm^{-1}). Using this shift of the Ge quantum well as well as the phonon confinement model, the biaxially compressive strain in the Ge quantum well is estimated to be ~1.25% (Fig. 1(b)).

Si/Ge heterojunction Light Emitting Diode

Fig. 2 shows EL spectra at different temperatures from the Ge quantum well MOS LED with 1 nm Si cap and the device size of 4×10^{-2} cm^2. The drive current is 50 mA at the gate voltage of -8 V. The electron-hole-plasma (EHP) recombination model can be used to fit the EL spectra. The apparent band gap is the low energy edge of the emission peak in the spectra. Device temperatures of 130 K, 210 K, and 320 K are obtained from the fitting of the EL line shapes, while the corresponding temperatures of cold finger in the EL measurement are 10 K, 150 K, and 300 K. The temperature difference is due to the device heating. The apparent energy gap extracted by the EHP model is ~0.52 eV (~2.4 μm), and ~0.56 eV (~2.2 μm) at the temperature of 320 K and 130 K, respectively. Due to the much smaller emission

energy as compared to strained Ge band gap, the 2-2.4 μm light emission is proposed to originate from the type-II Si/Ge heterojunction, i.e., the recombination of electron at Si conduction band and hole at Ge valence band (Fig. 3). To confirm the origin of ~0.52 eV emission, the quantum confinement energy of the Si cap and the Ge quantum well are calculated. There are small differences between the theoretic value and the measured data. The possible errors are the surface bending, the Ge phonon (36 meV) emission, and the interdiffusion of Si into Ge quantum well during the Si cap growth. The first two mechanisms reduce the photon emission energy, but the last mechanism increases the photon emission energy. The peak around 1.6 μm is the band edge emission of the Ge quantum wells, and is very weak due to the type II alignment of Si/Ge heterojunction. The Ge wells have a low electron concentration.

The strain enhancement is obtained by the mechanical setup in Fig. 4. The strain level can be obtained from Raman shift and agrees well with the ANSYS simulation and strain gauge measurement [3]. The red shift of EL spectra at 120 K under external tensile strain was found in the Si/Ge heterojunction (Fig. 5), as well as the bulk Si MOS LED (Fig. 6). The red shift of the bulk Si MOS LED is due to the downshift of conduction band and the upshift of the valence band. However, the red shift of the Si/Ge heterojunction MOS LED is smaller than the bulk Si LED (Fig. 7) due to the downshift of both Si conduction band and Ge valence band. The red shift is the difference of these two downshifts. Note the original compressive strain in Ge decreases by the external tensile strain.

Ge on Insulator (GOI) Photodetector

Fig. 8 shows the basic fabrication process of GOI MOS detector including hydrogen ion-implantation and direct wafer bonding techniques. The n-type, (001) germanium substrate was prepared as a "host" wafer. The hydrogen ions with a dose of 1×10^{17} cm^{-2} and the energy of 200 keV were implanted into the host wafer before bonding to form a deep weakened layer. On the other substrate, 80 nm thermal oxide was grown on the p-type Si substrate to form the "handle" wafer. The handle wafer and host wafer were hydrophilicly cleaned in the SC-1 clean and KOH : H_2O solution rinsed in de-ionized water, and initially bonded at the room temperature. The wafer pair were annealed to strengthen the chemical bonds between the interface of the two wafers and to induce layer transfer along the weakened hydrogen-implanted regions by H_2 blistering. The separated surfaces exhibit a root-mean-square roughness of ~7 nm after the H_2 blistering. The TEM image of GOI detector is shown in Fig. 9. Fig. 10 shows the typical dark and photo current of a GOI detector under different wavelength exposure. The fiber is pointed to the edge of the gate electrode and the photo-generated carriers can be collected by lateral diffusion/drift. The inset of Fig. 10 is the responsivity of GOI detector under light exposure. The GOI detector has the responsivity of 270, 200, and 50 mA/W at the wavelength of 850, 1310, and 1550 nm, respectively. The initial speed measurement of GOI detector without GSG RF pad shows 60 % enhancement as compared to bulk Ge detector. The higher speed is expected by using the GSG RF pad on the device. Fig. 11 shows the photo I-V characteristic of GOI MOS detector under external mechanical strain at 300 K. The photocurrent of the GOI and bulk Si detector under external strain enhance ~10% and ~15%, respectively as compared to the relaxed devices (The inset of Fig. 11) due to the band gap narrowing from the strain, while the change of dark current is smaller than 2 %. Fig. 12 shows the band diagram of a p-type Si detector under inversion bias. The deep depletion region is formed at inversion bias due to the tunneling of LPD oxide. The photoelectrons are generated in the deep depletion region, and are swept toward the gate electrode. The photoelectrons tunnel from the active layers to the Al gate electrode through the trap-assisted tunneling of LPD oxide. The dark current is mainly determined by the generation rate of minority carrier via interface states at oxide/semiconductor interface. Therefore, the band gap narrowing due to strain has less effect on the dark current as compared to the photo current.

Summary

In summary, the 2 μm Si/Ge heterojunction emission LED, and the high-efficient and high-speed GOI MOS detector are reported for the first time. By the proper design of the strain mechanism, it can possibly further extend the wavelength to mid-infrared for the light emission and enhances the responsivity for detection. The high performance makes it feasible to integrate optoelectronic devices into the Si chip for future applications. Both strain-enhanced light emission and detection from Si/Ge metal-oxide-semiconductor devices are demonstrated.

Acknowledgments

The support of Raman measurement by Prof. Chih-Ta Chia at the National Taiwan Normal University is highly appreciated. This work is supported by National Science Council of ROC under contract Nos. 93-2215-E-002-003 and 93-2215-E-002-017, and US air force (AOARD-04-4072).

References

(1) C. W. Liu et al., "Light emission and detection by metal oxide silicon tunneling diodes," *IEDM Tech. Dig.*, pp.749-752, 1999.
(2) B.-C. Hsu et al., "High Efficient 820 nm MOS Ge Quantum Dot Photodetectors for Short-Reach Integrated Optical Receivers with 1300 and 1550 nm Sensitivity," *IEDM Tech. Dig.*, pp.91-94, 2002.
(3) M. H. Liao, M.-J. Chen, T. C. Chen, P.-L. Wang, and C. W. Liu, "Electroluminescence from metal/oxide/strained-Si tunneling diodes," *Appl. Phys. Lett.*, vol. 86, p. 223502, 2005.
(4) T. C. Chen, W. Z. Lai, C. Y. Liang, M. J. Chen, L. S. Lee, and C. W. Liu, "Light emission from Al/HfO_2/Siliocn diodes," *Journal of Applied Phys.*, vol. 95, p. 6486, 2004.
(5) C. W. Liu, S. Maikap, and C.-Y. Yu, "Mobility-Enhancement Technologies," *IEEE Circuits and Devices Magazine*, p. 21, May/June, 2005.

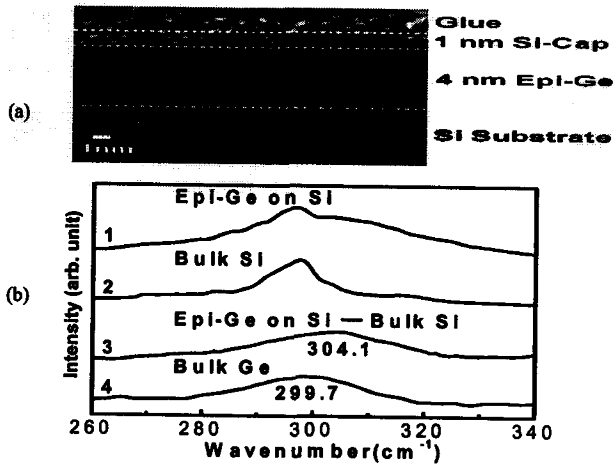

Fig. 1 (a) The cross-sectional transmission electron micrograph of the as-grown Ge quantum well on (100) Si. (b) The Raman spectra of epi-Ge on Si (curve 1), Si substrate (curve 2), pure Ge layer without Si substrate interference (curve 3), and the bulk Ge wafer (curve 4). The blue shift of Ge-Ge peak of curve 3 w.r.t. curve 4 indicates the compressive strain of ~1.25%.

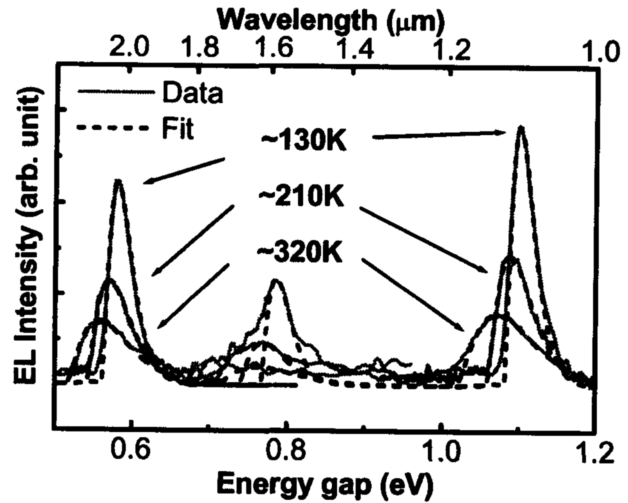

Fig. 2 The electroluminescence spectra of strained Ge/Si heterojunction MOS LED with the fitting curves of the electron-hole plasma recombination model at 130, 210, and 320 K. Three peaks could be corresponding to the Si cap emission, epi-Ge emission, and the Si/Ge heterojunction emission.

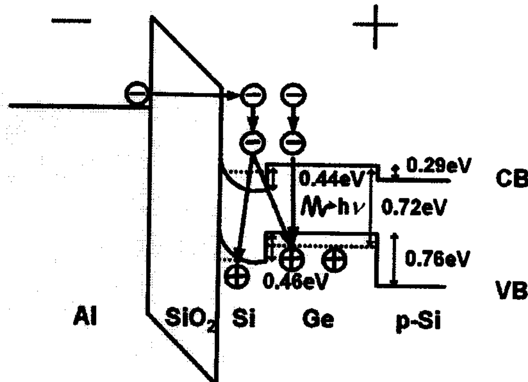

Fig. 3 The schematic band diagram of the strained Ge quantum well (4 nm) device with a Si cap (1 nm) for NMOS tunneling diode. The 2 μm emission is proposed from the transition of the Si conduction band to the Ge valence band.

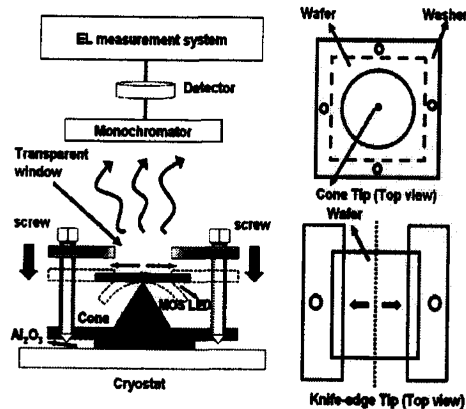

Fig. 4 Schematic diagram of the mechanical setup to apply biaxially and uniaxially mechanical strain in the low temperature cryostat.

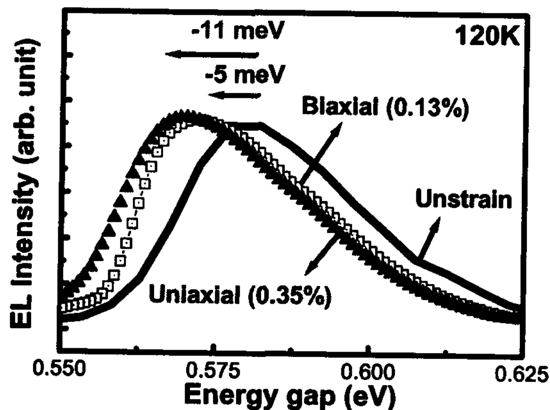

Fig. 5 The EL spectra of a strained Ge/Si heterojunction MOS LED under external 0.13% biaxial tensile strain and 0.35% uniaxial tensile strain at 120K.

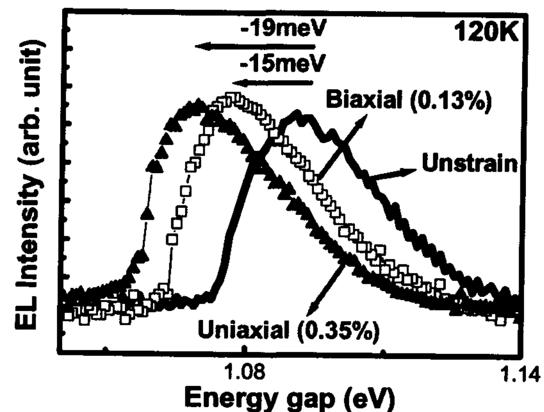

Fig. 6 The EL spectra of a strained Si MOS LED under external 0.13% biaxial tensile strain and 0.35% uniaxial tensile strain at 120K.

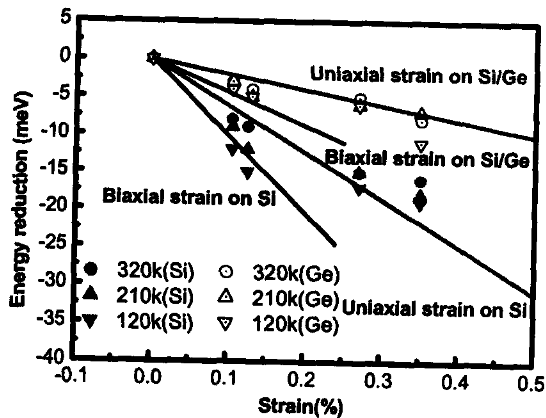

Fig. 7 The theoretical emission energy reduction and the red shift data from EL measurement under external strain. The red shift of strained Ge/Si heterojunction is due to the relative down shift of Si conduction band edge and Ge valence band edge, and is smaller than that of bulk Si.

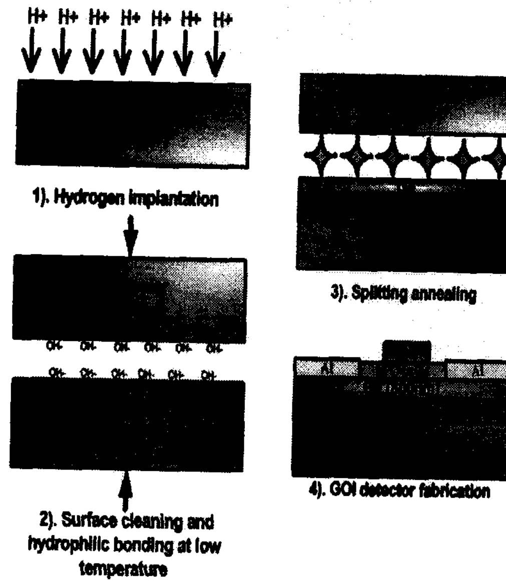

Fig. 8 The fabrication of Ge on insulator (GOI) MOS detector.

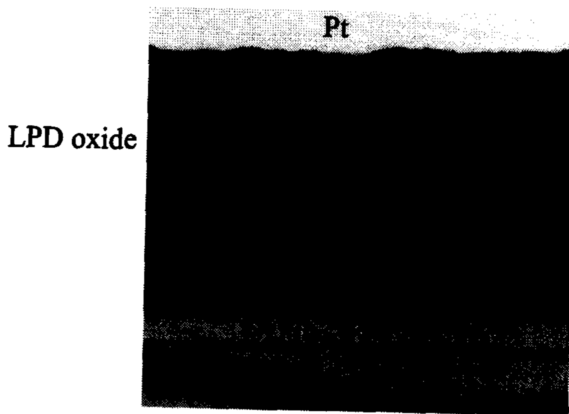

Fig. 9 The cross-sectional transmission electron micrograph of the GOI detector.

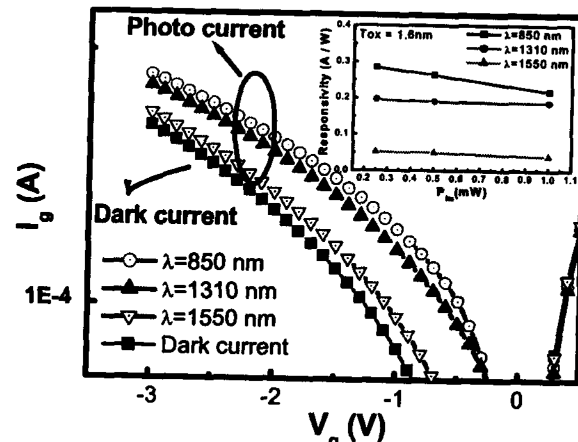

Fig. 10 The dark and photo I-V characteristic and the responsivity vs. different input power of a GOI detector under 850 nm, 1310 nm, and 1550 nm lightwave exposure.

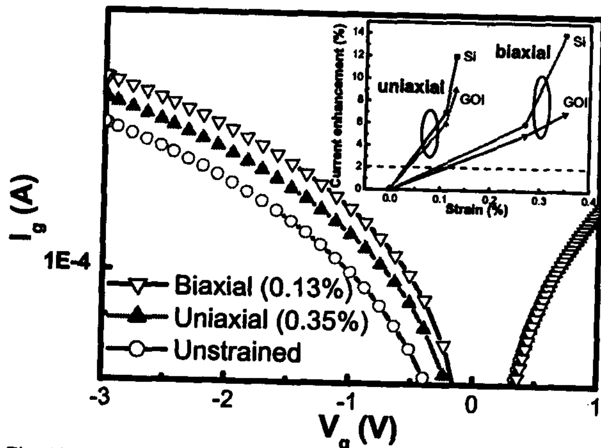

Fig. 11 The photo I-V characteristic (850 nm exposure) of GOI detector under external tensile strain at 300K. The inset of Fig. 11 shows the photo current enhancement of GOI and Si MOS detector vs. mechanical strain. The change of dark current is smaller than 2%.

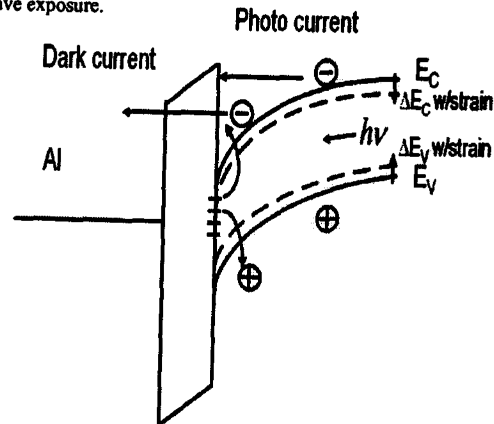

Fig. 12 The band diagram of p-Si photodetector under inversion bias. The photo-generated electrons tunnel through LPD oxide and can be enhanced by band gap narrowing. The dark current is determined by the Dit, and hence band gap narrowing due to strain has less effect on dark current.